THE JOURNAL OF PHYSICAL CHEMISTRY B

ARTICLE

pubs.acs.org/JPCB

Investigations on Ferroelectric Liquid Crystal by High Resolution TEM and Solid State ^{13}C NMR

Yongxia Zhao, Yanqin Yang, Jingwei Xu,* Wei Yang,* Yunchun Zhou, Zijiang Jiang, and Xin Ge

The State Key Laboratory of Electroanalytic Chemistry, Chinese Academy of Sciences, Changchun Institute of Applied Chemistry, Changchun, 130022, People's Republic of China

Supporting Information

ABSTRACT: In order to investigate the structural and dynamical properties of ferroelectric liquid crystal (FLC) in different phases a model compound [4-(3)-(*S*)-methyl-2-(*S*)-chloropentanoyloxy)]-4′-nonyloxy-biphenyl (3M2CPNOB) is synthesized. High resolution transmission electron microscopy (HR-TEM) is applied to observe the morphology of 3M2CPNOB and temperature-dependent solid state ^{13}C NMR to record ^{13}C chemical shifts at different phases. A liquid nitrogen quenching method is used to maintain the conformation of the mesophases for HR-TEM experiments. TEM images show that all the smectic A (SmA), smectic C* (SmC*) and crystalline phases have lamellar morphology. The interplanar distances in the crystalline phase are smaller than those in SmA and SmC* phases because of denser arrangement of the molecules. Both ^{13}C chemical shifts and line shape vary with different phases. The experimental results suggest that SmC* phase as an intermediate occurs in the anisotropy transition process from SmA to crystalline phase, the helical structure of the SmC* phase unwinds in the magnetic field and the conformations of the SmA and isotropic phase are very similar.

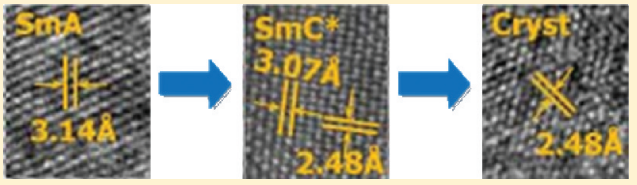

1. INTRODUCTION

Chiral ferroelectric liquid crystal (FLC) was first discovered by Meyer and co-workers in 1975.[1] For symmetry reasons chiral tilted smectic phases of FLC possess a spontaneous polarization P_S which is perpendicular to the molecular "tilt plane". Their potential applications in the fast electro-optic devices, flat panel displays, and many other fields have attracted great interest over the last decades.[2,3] The physical properties of FLC, such as molecular reorientation during electro-optic switching[4,5] and dielectric properties[6−8] etc. have been widely studied. The distances between oriented molecules were typically measured by powder X-ray diffraction (XRD)[9−11] and thus the microscopic arrangements of the molecules were derived. As we know, little direct observation of the microscopic arrangements was reported.[12,13] This information is of paramount importance not only for establishing property-structure correlations but also for designing future materials.

The modern transmission electron microscopy (TEM) techniques are capable of observing the microstructures at subnanometer levels, which is the scale of the molecular distances in liquid crystals (LCs). However, the fact of the mesophases' temperature above the room temperature slows down the application of TEM on thermotropic LCs. In order to directly observe thermotropic LCs, Costello et al.[14] quickly froze the samples to −170 °C and the result showed that the blue phase of the LC was maintained by rapid freeze fracture method. This technique was also applied in observing varied LCs by Hudson[15−17] and co-workers.

In the past decades, solid state nuclear magnetic resonance (NMR) has emerged as a powerful tool for the characterization of molecular structures and conformations of mesogens in the smectic phases to investigate the structure,[18] orientational ordering,[19] and dynamics[20] of low molecular weight LCs.[21−25] Compared to solid state ^{2}H NMR, the ^{13}C NMR could acquire spectra of the mesophases without labeling in the LC molecules. The structural and dynamical information of each phase could be obtained by the resolved signals.

In this work, TEM together with a simple freezing method was used to observe the structure of a FLC formed by [4-(3)-(*S*)-methyl-2-(*S*)-chloropentanoyloxy)]-4′-nonyloxy-biphenyl (3M2CPNOB, Scheme 1). The microstructure of the FLC at subnanometer scale was directly observed. In addition, the temperature-dependent solid state ^{13}C NMR technique was used to study the dynamical behavior of the phase transition procedures and conformations of 3M2CPNOB in different phases.

2. EXPERIMENTAL SECTION

2.1. Synthesis of 3M2CPNOB. [4-(3)-(*S*)-Methyl-2-(*S*)-chloropentanoyloxy)]-4′-nonyloxy-biphenyl was synthesized following the procedure described previously (see Supporting Information).[26]

2.2. Differential Scanning Calorimetry (DSC). The thermal properties of 3M2CPNOB between 30 and 70 °C were determined by DSC (Pyris Diamond, Perkin-Elmer 7) with repeated heating−cooling cycles at a heating and cooling rate of 2 °C/min.

Received: August 14, 2011
Revised: September 27, 2011
Published: October 03, 2011

Scheme 1. Chemical Structure of 3M2CPNOB with Indicated Carbon Site Labels

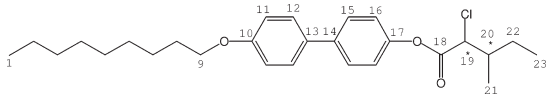

2.3. Polarized Optical Microscopy (POM). The POM images were captured using a polarized optical microscope (Shanghai Changfang Optical Instrument Co., Ltd., China) equipped with a digital color video camera. The temperatures of FLC samples were controlled by a hot-stage (Changzhou Nuohai Electronic Co., Ltd., China). Samples heated to isotropic phase (Iso) were introduced into the LC cell by capillary forces first, and then cooled to 55 °C, 45 and 25 °C respectively at a rate of 2 °C/min. The LC cell was comprised of two pieces of CaF_2 plates. The inner surface of each plate was coated with a thin layer of polyimide unidirectionally rubbed in order to induce a homogeneous orientation of the FLC molecules. The CaF_2 plates were separated by a polycarbonate spacer with a thickness of 2.8 μm.

2.4. High Resolution Transmission Electron Microscopy (HR-TEM). The HR-TEM imaging was operated on a Philips-FEI Tecnai F20 microscopy (Philips, The Netherlands) at an accelerating voltage of 200 kV. Low-dose procedures were used for this material to avoid beam damaging[16,27,28] on the organic molecules. All of the images were taken in an appropriate defocus condition to increase the image contrast.[29]

To prepare samples for HR-TEM experiments, 3M2CPNOB was dispersed in anhydrous ethanol (~0.1 wt %) and then submitted to ultrasonication for better dispersion. A drop of suspension was deposited onto a 200 mesh copper lacey support film (Beijing Xinxingbairui Technology Co., Ltd., China) that was covered with a carbon film. After the ethanol volatilized absolutely, the 3M2CPNOB on the lacey support film was heated to isotropic phase using a hot-stage. Then the samples were cooled to smectic A (SmA), smectic C* (SmC*), and crystalline phases, respectively, at the same rate as the DSC method and kept for 5 min at the desired temperatures. Then the samples were quickly plunged into liquid nitrogen. As references, the samples in the LC cell were heated and cooled simultaneously at the same hot-stage and followed the liquid nitrogen quenching procedures also. The POM images before and after quenching were compared to ensure that the quenching treatment kept the structures of the FLC at the desired temperatures.

2.5. Solid State ^{13}C NMR Measurements. The temperature-dependent solid state ^{13}C NMR experiments were carried out on a Bruker AVANCE III 400 WB spectrometer equipped with a 4 mm standard bore CP/MAS (cross-polarization and magic angle spinning) probehead whose X channel was tuned to 100.62 MHz for ^{13}C and the other channel was tuned to 400.18 MHz for broad band ^{1}H decoupling, using a magnetic field of 9.39 T. The sample packed in the ZrO_2 rotor closed with Kel-F cap was heated by the nitrogen flow at a rate of 935 L/h. All of the spectra were taken as static spectra using the CP/HPDEC (cross-polarization and high power decoupling) technique. First the sample was heated to isotropic phase at 65 °C and then continuously cooled to the SmA, SmC*, and crystalline phases with a rate of 1 °C/min. At each data point, the temperature was stabilized for 10 min before collecting the spectra. A total of 100 scans were recorded with 8 s recycle delay for each sample. All ^{13}C chemical shifts were referenced to the resonances of adamantane standard (δ = 29.5 ppm). The temperature calibration was implemented using the known phase transition temperatures of the FLC and the fluctuation of the temperature was approximate to ±1 °C.[6,19]

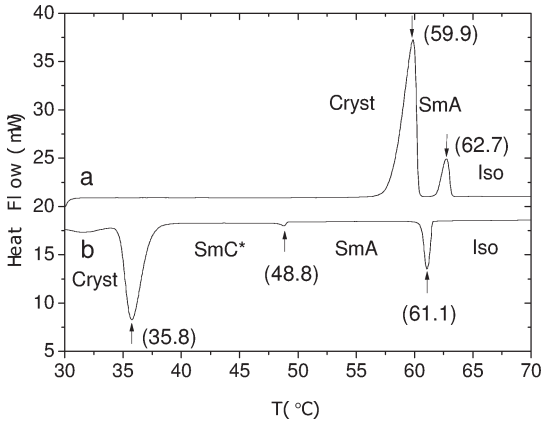

Figure 1. DSC plot of heating (a) and cooling (b) curves of 3M2CPNOB with a temperature change rate of 2 °C/min. Vertical arrows indicate the phase transition points, and the numbers in the parentheses are the corresponding phase transition temperatures. Phases at each stage are labeled.

3. RESULTS AND DISCUSSION

3.1. The DSC. The DSC measurements (Figure 1) indicate that 3M2CPNOB undergoes only one LC phase during the transition of the crystal phase (Cryst) to the isotropic phase by mild heating. The transition points from the crystal phase to LC phase and further to isotropic phase are at 59.9 and 62.7 °C, respectively. However, during the reverse process of cooling, it undergoes two LC phases. In addition to the isotropic-to-liquid crystal transition at 61.1 °C and liquid crystal-to-crystal transition at 35.8 °C, a small but evident enthalpy release is observed when the FLC is cooled to about 48.8 °C, which suggests a transition between two different LC phases. POM images show that the mesophase in the heating process is SmA while the phases in the cooling process are SmA and SmC*, respectively.

3.2. The POM. The POM images from the cooling process are shown in Figure 2. At 55 °C, 3M2CPNOB presents a fan-shaped texture (Figure 2a), which is a typical texture of SmA phase. At 45 °C, the texture is similar to that at 55 °C, except that some screw threads appear (Figure 2b), which is inherent to the SmC* phase. The POM image at room temperature shows a typical texture of the crystalline phase (Figure 2c).

The images of crystalline phase before and after quenching are unchanged (Figure 2c,f). However, images of quenched samples in SmA and SmC* phases are obviously different (Figure 2d,e). Further analysis suggests that the texture patterns of the LC phases are maintained after quenching but these images provide more detailed structures. This difference mainly arises from the thermal motion. At 45 or 55 °C, the molecular tumbling is much greater than that at 25 °C, which results in a lowered-resolution. At 25 °C, the step-like layer structures in smectic phases in the quenched samples are observed more clearly compared to that at higher temperatures. In addition, the structure arrangement in SmC* has more regularity than that in SmA phase. All of the results indicate that the structural characteristics are maintained after liquid nitrogen quenching process.

3.3. The HR-TEM. In order to investigate the structure of different phases at molecular level, HR-TEM was applied on the quenched samples. It is well-known that both the SmA and SmC* phases have layered structure. The crystalline phase that crystallized from a smectic mesophase may also have the same layered structure.[16,17] Consistently, the TEM images of 3M2CPNOB (Figure 3) clearly show that all the SmA, SmC* and crystalline phases present lamellar morphology, and the layers are approximately parallel to the carbon substrate.

In addition to the orientational order, the assembly of LC at smectic phase also possesses one-dimensional positional order in the layer.[17] The calculated molecular length of 3M2CPNOB is about 26.2 Å (by Chem3D Ultra, MM2 method), which is much longer than the interplanar distances obtained from the power spectra (Figure 4e−g), suggesting the incident direction of the electron beam is approximately parallel to the molecular long axis in these images.

In HR-TEM picture (Figure 4a), 2D lattice fringes are observed for the SmA phase. In this phase, molecules assemble in parallel lines, which suggests the ordered-structure in layers.

Interplanar distances can be calculated from power spectra which result from selected HR-TEM squares by Fast Fourier transform. In Figure 4e that is transformed from 4a, interplanar distances at four directions are calculated to be $d1$ = 2.89 Å, $d2$ = 2.80 Å, $d3$ = 3.14 Å, and $d4$ = 1.80 Å, respectively. The first three values fit with the distance between two lattice fringes detected directly from the HR-TEM pictures. They give an average intermolecular distance of 2.94 Å. The short distance of 1.80 Å is more likely an intramoleclular one but we cannot assign it to specific groups yet.

The molecular organization in the SmC* phase (Figure 4b) is more ordered than that in the SmA phase. Very clear and regular 2D lattice fringes are observed. The ordered arrangement allows us to distinguish each molecular unit in the image. In each unit, brighter and relatively darker dots are closely located in one orientational lattice fringe, likely arising from the two benzene rings of the biphenyl group in 3M2CPNOB. The brightness difference suggests that the two benzene rings are not located at the same plane. The regular dot arrangement of brighter−darker cycles (Figure 4d) suggests that 3M2CPNOB aligned by its biphenyl part in a layer and the lengthy tails point out toward the same direction.

From Figure 4f that is transformed from 4b, six distances are obtained, which are $d1$ = 3.07 Å, $d2$ = 1.90 Å, $d3$ = 4.03 Å, $d4$ = 2.48 Å, $d5$ = 3.83 Å, and $d6$ = 1.89 Å, respectively. As the observations are in the SmA phase, the short distances of 1.90 and 1.89 Å are likely intramolecular. The average interplanar distance is 3.35 Å for the SmC* phase.

In crystalline phase (Figure 4c), similar 2D lattices are observed as that in smectic phases. However, from Figure 4g that is transformed from 4c, the interplanar distances with $d1$ = 2.46 Å, $d2$ = 2.44 Å, and $d3$ = 2.48 Å at three directions are quite uniform. The longer distances above 3 Å are not observed. The results show that the molecules in the crystalline phase arrange denser than that in the smectic phases.

The interplanar distances observed in SmC* contain both the distance of 3.07 Å that closes to the SmA phase and 2.48 Å that closes to the crystalline phase. This result suggests a transition mechanism from SmA phase to the crystalline phase. That is, reducing the interplanar distance from ~3 Å in SmA phase to ~2.5 Å in crystalline phase does not occur simultaneously in all directions. Indeed, the rearrangement of the 2D lattice is carried out at one direction first (d4 direction in Figure 4f). This anisotropy rearrangement converts the SmA phase into SmC* phase. The longer distances ~4 Å observed in SmC* phases correlate to the diagonal line of a 2.5 × 3 Å rectangle ($2.5^2 + 3^2 = 15.25 \approx 3.91^2$).

Overall, the molecular organizations of 3M2CPNOB at different phases are directly observed at subnanometer scales. In smectic layers, the molecules arrange orderly like that in crystal. The less crowded arrangements in LC phases are consistent with their liquidity. Comparing to the other techniques such as powder XRD in which only two peaks are found in the SmC* phase, the sharp peak indicates the long-range order of layers,

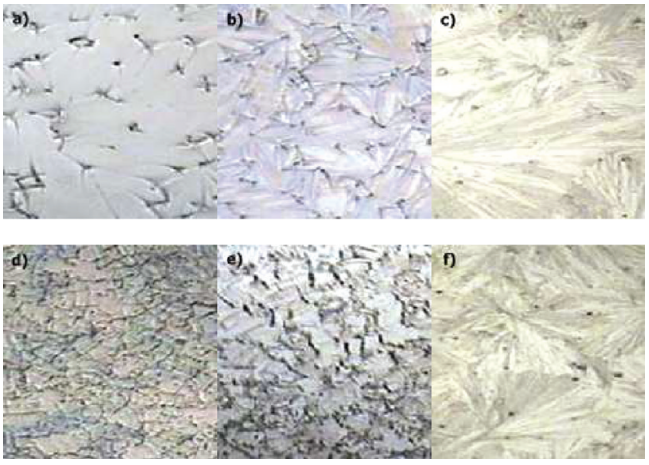

Figure 2. POM photographs of 3M2CPNOB on cooling from isotropic state to (a) 55 °C, (b) 45 °C, and (c) 25 °C. The images of (d), (e), and (f) are quenched from (a), (b), and (c) in liquid nitrogen, respectively.

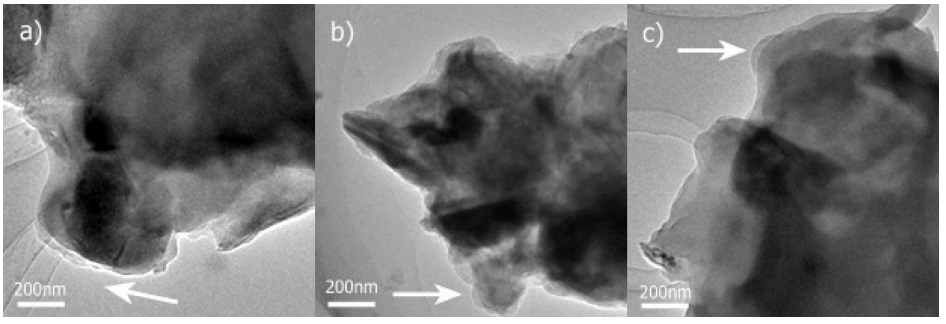

Figure 3. TEM images of 3M2CPNOB (a) SmA phase quenched at 55 °C, (b) SmC* phase quenched at 45 °C, and (c) unquenched crystalline phase at 25 °C. The arrow in each picture indicates the lamellar morphology of the corresponding phase.

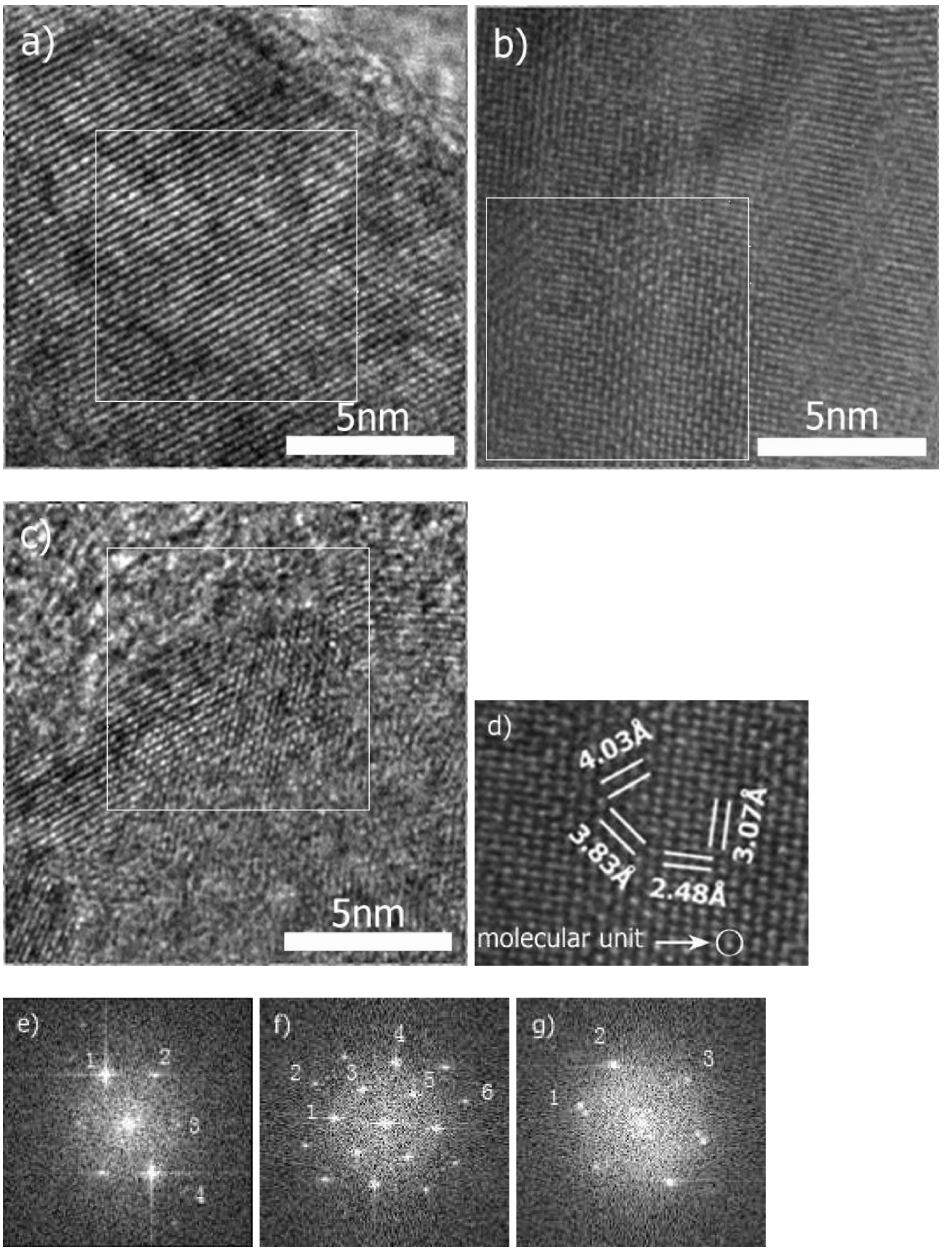

Figure 4. HR-TEM images of 3M2CPNOB (a) SmA phase quenched at 55 °C, (b) SmC* phase quenched at 45 °C, (c) unquenched crystalline phase at 25 °C, and (d) the local enlarged view of Figure 4b. Images (e), (f), and (g) are the corresponding power spectra of (a), (b), and (c), respectively.

meanwhile the halo peak gives information about the translational short-range order of molecules in the layer. The intermolecular distance given by powder XRD is only the average intermolecular distances.[30,31] HR-TEM demonstrates its advantage by the capability of providing specific intermolecular distances at different directions. The results demonstrate the anisotropy during the phase transition from SmA phase to crystalline phase. To our knowledge, the images are first reported to show the microstructure of FLC at molecular level.

3.4. The Solid State ^{13}C NMR Spectra. Temperature-dependent solid state ^{13}C NMR spectra of 3M2CPNOB are shown in Figure 5. The assignment of the ^{13}C spectrum in the isotropic phase (Figure 5a) has been carried out on the basis of solution-state ^{1}H, ^{1}H−^{13}C HMQC NMR spectra and the NMR spectra of the other LC that has similar structure.[32]

Compared to the isotropic ^{13}C spectrum, the relative position of each peak in the SmA phase is almost unchanged and only the peak width becomes broad slightly because of the decreased mobility in the SmA phase, which indicates that the conformations of the SmA and isotropic phases are very similar. When cooling to about 49 °C, that is near the SmA-to-SmC* phase transition temperature, some new peaks that belong to the following SmC* phase appear. Meanwhile, the peaks of the SmA phase preserve. Moreover, all of the aromatic, carbonyl, and alkyl signals are included in the new peaks, which suggest that the conformations of the core and tail parts change simultaneously in the phase transition process. With further decrease of temperature, the sample completely transforms to the SmC* phase. The chemical shifts of the aromatic and carbonyl carbons (from 125 to 225 ppm) markedly shift downfield as is usually

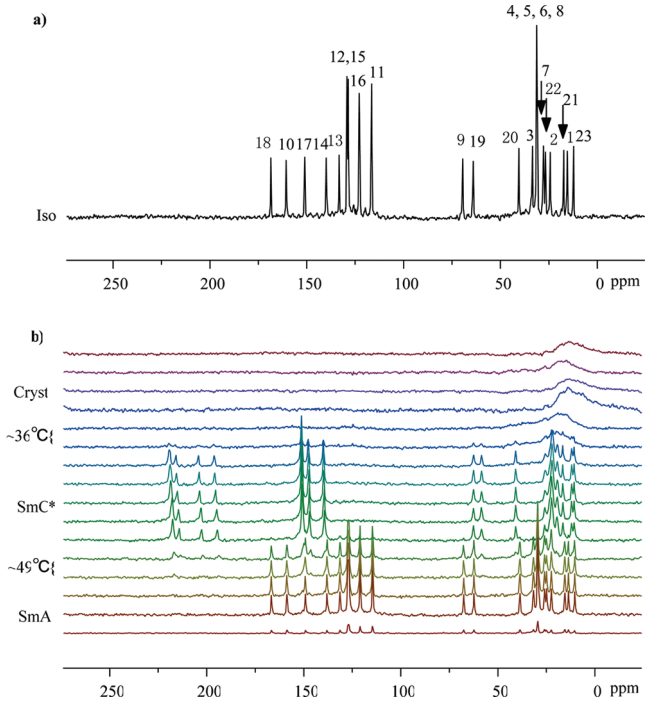

Figure 5. Series of static ^{13}C NMR spectra of 3M2CPNOB (a) ^{13}C NMR spectrum in the isotropic phase at 65 °C, (b) ^{13}C NMR spectra in the LC and crystalline phases at different temperatures. Phases and phase transition temperatures are labeled.

found when the helix structure of the SmC* phase is unwound by the magnetic field.[6,19] By decreasing the temperature within the SmC* range, the movement continuously increases due to the total unwinding of the helical structure. The field to unwind a helix is inversely proportional to the length of its pitch.[33] It is likely that the helical pitch of 3M2CPNOB is long enough so that the unwinding could be completed under the magnetic field of 9.39 T. Because of the total unwinding of the helical structure the tilt angle of the SmC* phase cannot be fixed by the analysis of chemical shift variations with temperature.[6,19] In addition, the peaks of the tail carbons (from 0 to 35 ppm) broaden and overlap each other when entering into the SmC* phase, which indicates the further decreased mobility of the sample. The chemical shifts of the chiral carbons C19, C20 and the alkoxy carbon C9 exhibit different variations when entering into the SmC* phase, the signals of C9, C19 move upfield meanwhile the C20 goes downfield. After that, they all keep constant frequency within the SmC* phase. This phenomenon can be attributed to the change of the conformation at the phase transition process instead of the continuously increase of the orientational order of the fragments.[34] When the temperature goes down to about 36 °C that corresponding to the SmC*-to-Cryst phase transition temperature, the intensity of the signals (from 35 to 225 ppm) becomes very weak and the peaks of the tail carbons (from 0 to 35 ppm) become very broad and overlap each other seriously. By entering the crystal phase only a very broad signal of the tail carbons (from 0 to 35 ppm) can be seen.

From the temperature-dependent ^{13}C NMR spectra (Figure 5b) we can distinguish each phase easily since the spectra in each phase different from each other both in the line shape and the chemical shifts. The phase transition processes of SmA-to-SmC* and SmC*-to-Cryst could also be clearly seen. The characteristic is that the sample undergoes a biphasic region (about 3 °C) throughout the process.

4. CONCLUSIONS

In this study, we demonstrate that liquid nitrogen quenching is capable of maintaining the conformation of the LC phases for TEM experiments. The TEM results show that all of the SmA, SmC*, and crystalline phases have lamellar morphology. Interplanar distances are also calculated from the HR-TEM images, and the results indicate that the interplanar distances in the crystalline phase are smaller than those in SmA and SmC* phases because of denser arrangement of the molecules. The SmC* phase as an intermediate occurs in the anisotropy transition process from SmA to crystalline phase. In SmC* phase, molecular units comprised of a brighter dot and a relatively darker dot are observed, likely to be the biphenyl unit of the molecule.

The temperature-dependent solid state ^{13}C NMR spectra clearly provide phase transition processes. The characteristic is that the sample undergoes a biphasic region (about 3 °C) throughout the processes. Both ^{13}C chemical shifts and the line shape vary with different phases. The abruptly increased chemical shifts of the aromatic and the carbonyl carbons imply the unwinding of the helical structure of the SmC* phase in the magnetic field and further total unwinding with the decreasing of the temperature in the SmC* range. The spectra in the SmA phase are very similar to that in the isotropic phase, which suggests that the conformations in these two phases are very similar.

■ ASSOCIATED CONTENT

Supporting Information. Detailed synthetic procedures and characterization of [4-(3)-(*S*)-methyl-2-(*S*)-chloropentanoyloxy)]-4′-nonyloxy-biphenyl. This material is available free of charge via the Internet at http://pubs.acs.org.

■ AUTHOR INFORMATION

Corresponding Author

*Phone: +86-431-85262643; Fax: +86-431-85262649; E-mail: jwxu@ciac.jl.cn (J.X.). Phone: +86-431-85262354; E-mail: yangwei@ciac.jl.cn (W.Y.).

■ ACKNOWLEDGMENT

The authors would like to thank Changchun Fangguan Electronics Technology Co., Ltd. (China) for the help in making liquid crystal cells.

■ REFERENCES

(1) Meyer, R. B.; Liebert, L.; Strzelecki, L.; Keller, P. *J. Phys., Lett.* **1975**, *36*, L169.
(2) Lagerwall, S. T. In *Ferroelectric and Antiferroelectric Liquid Crystals*; Wiley-VCH: Weinheim, Germany, 2007; Chapter 9.
(3) Lagerwall, J. P. F; Giesselmann, F. *ChemPhysChem* **2006**, *7*, 20.
(4) Jang, W. G. *J. Korean Phys. Soc.* **2001**, *39*, 296.
(5) Hemine, J.; Daoudi, A.; Legrand, C.; Isaert, N.; El kaaouachi, A.; Nguyen, H. T. *Physica B* **2007**, *399*, 60.
(6) Bubnov, A.; Domenici, V.; Hamplova, V.; Kaspar, M.; Veracini, C. A.; Glogarova, M. *J. Phys.:Condens. Matter* **2009**, *21*, 1.
(7) Domenici, V.; Geppi, M.; Veracini, C. A.; Zakharov, A. V. *J. Phys. Chem. B* **2005**, *109*, 18369.

(8) Geppi, M.; Marini, A.; Veracini, C. A.; Urban, S.; Czub, J.; Kuczynski, W.; Dabrowski, R. *J.Phys. Chem. B* **2008**, *112*, 9663.
(9) Yoshizawa, A.; Nishiyama, I.; Kikuzaki, H.; Ise, N. *Jpn. J. Appl. Phys.* **1992**, *31*, L860.
(10) Doi, T.; Sakurai, Y.; Tamatani, A.; Takenaka, S.; Kusabayashi, S.; Nishihata, Y.; Terauchi, H. *J. Mater. Chem.* **1991**, *1*, 169.
(11) Stamatoff, J.; Cladis, P. E.; Guillon, D.; Cross, M. C.; Bilash, T.; Finn, P. *Phys. Rev. Lett.* **1980**, *44*, 1509.
(12) Mao, G. P.; Wang, J. G.; Ober, C. K. *Chem. Mater.* **1998**, *10*, 1538.
(13) Durst, H.; Voigt-Martin, I. G. *Makromol. Chem.* **1986**, *7*, 785.
(14) Costello, M. J. *Phys. Rev. A* **1984**, *29*, 2957.
(15) Hudson, S. D. *Curr. Opin. Colloid. In.* **1998**, *3*, 125.
(16) Jung, H. T.; Hudson, S. D. *Macromolecules* **1998**, *31*, 637.
(17) Hudson, S. D.; Lovinger, A. J. *Macromolecules* **1994**, *27*, 3357.
(18) Das, B.; Grande, S.; Weissflog, W.; Eremin, A.; Schroder, M. W.; Pelzl, G.; Diele, S.; Kresse, H. *Liq. Cryst.* **2003**, *30*, 529.
(19) Dong, R. Y.; Geppi, M.; Marini, A.; Hamplova, V.; Kaspar, M.; Veracini, C. A.; Zhang, J. *J. Phys. Chem. B* **2007**, *111*, 9787.
(20) Satoh, H.; Hiraoka, K.; Uematsu, Y. *Ferroelectrics* **1998**, *212*, 99.
(21) Domenici, V.; Geppi, M.; Veracini, C. A. *Prog. Nucl. Magn. Reson. Spectrosc.* **2007**, *50*, 1.
(22) Domenici, V. *Pure Appl. Chem.* **2011**, *83*, 67.
(23) Marini, A.; Prasad, V.; Dong, R. Y. In *Nuclear Magnetic Resonance Spectroscopy of Liquid Crystals*; Dong, R. Y., Ed.; World Scientific Publishing Co.: Singapore, 2009; Chapter 12.
(24) Cifelli, M.; Domenici, V.; Marini, A.; Veracini, C. A. *Liq. Cryst.* **2010**, *37*, 935.
(25) Marini, A.; Domenici, V. *Ferroelectrics* **2010**, *395*, 46.
(26) Sakurai, T.; Mikami, N.; Higuchi, R. I.; Honma, M.; Ozaki, M.; Yoshino, K. *J. Chem. Soc., Chem. Commun.* **1986**, 978.
(27) Sagalowicz, L.; Acquistapace, S.; Watzke, H. J.; Michel, M. *Langmuir* **2007**, *23*, 12003.
(28) Voigt-Martin, I. G.; Simon, P.; Garbella, R. W. *Makromol. Chem* **1991**, *12*, 285.
(29) Zhao, N.; Botton, G. A.; Zhu, S. P.; Duft, A. *Macromolecules* **2004**, *37*, 8307.
(30) Dobiasova, L.; Sichova, H.; Valvoda, V. *Powder Diffr.* **2003**, *18*, 293.
(31) Obadovic, D. Z.; Vajda, A.; Garic, M.; Bubnov, A.; Hamplova, V.; Kaspar, M.; Fodor-Csorba, K. *J. Therm. Anal. Calorim.* **2005**, *82*, 519.
(32) Poon, C. D.; Fung, B. M. *J. Chem. Phys.* **1989**, *91*, 7392.
(33) deGennes, P. G. *The Physics of Liquid Crystals*; Oxford University: London, 1974.
(34) Marini, A.; Domenici, V. *J. Phys. Chem. B* **2010**, *114*, 10391.